Characterizing the human APOE epsilon 4 knock-in transgene in female and male rats with multimodal magnetic resonance imaging

Praveen Kulkarni
Northeastern University
Simone Grant
University of California Davis
Thomas Morrison
Northeastern University
Xuezhu Cai
Northeastern University
Sade Iriah
Northeastern University
Bruce Kristal
Brigham and Women's Hospital
Jennifer Honeycutt
Northeastern University
Heather Brenhouse
Northeastern University
Jochen Hartner
Horizon Discovery Group plc
Dan Madularu
Northeastern University
Craig Ferris (c.ferris@neu.edu)
Northeastern University https://orcid.org/0000-0001-9744-5214

Research

Keywords: voxel-based morphometry, diffusion weighted imaging, indices of anisotropy, resting state BOLD fMRI, sex differences, deep cerebellar nuclei, default mode network, reticular activating system

Posted Date: March 19th, 2020

DOI: https://doi.org/10.21203/rs.3.rs-18040/v1

Version of Record: A version of this preprint was published at Brain Research on November 1st, 2020. See the published version at https://doi.org/10.1016/j.brainres.2020.147030.

Abstract

Background: The APOE ε4 genotype is the most prevalent genetic risk for Alzheimer's disease (AD). Women carriers of ε4 have higher risk for an early onset of AD than men. Human imaging studies suggest apolipoprotein E4 may affect brain structures associated with cognitive decline in AD many years before disease onset. It was hypothesized that female APOE ε4 carriers would present with decreased cognitive function and neuroradiological evidence of early changes in brain structure and function as compared to male carriers.

Methods: Six-month old wild-type (WT) and human APOE ε4 knock-in (TGRA8960), male and female Sprague Dawley rats were studied for changes in brain structure using voxel-based morphometry, alteration in white and gray matter microarchitecture using diffusion weighted imaging with indices of anisotropy, and functional coupling using resting state BOLD functional connectivity. Images from each modality were registered to, and analyzed, using a 3D MRI rat atlas providing site-specific data on over 168 different brain areas.

Results: Quantitative volumetric analysis revealed areas involved in memory and arousal were significantly different between ε4 and wild-type (WT) females, with few differences between male genotypes. Diffusion weighted imaging showed few differences between WT and ε4 females, while male genotypes showed significant different measures in fractional anisotropy and apparent diffusion coefficient. Resting state functional connectivity showed ε4 females had greater connectivity between areas involved in cognition, emotion, and arousal compared to WT females, with male ε4 showing few differences from controls. Interestingly, male ε4 showed increased anxiety and decreased performance in spatial and episodic memory tasks compared to WT males, with female genotypes showing little difference across behavioral tests.

Conclusion: The sex differences in behavior and diffusion weighted imaging suggest male carriers of the ε4 allele may be more vulnerable to cognitive and emotional complications compared to female carriers early in life. Conversely, the data may also suggest that female carriers are more resilient to cognitive/emotional problems at this stage of life perhaps due to altered brain volumes and enhanced connectivity.

Introduction

Apolipoprotein E (ApoE) is found throughout the body, and is known for its role in regulating protein metabolism and lipid transport between cells [1]. ApoE is synthesized in the brain by astrocytes, microglia, and select neurons [1, 2]. The gene (APOE) that codes for ApoE is polymorphic and has three common alleles (i.e., ε2, ε3, and ε4) that code for three protein isoforms (i.e., ApoE2, ApoE3, and ApoE4, respectively) [3]. The APOE genotypes have become a major focus in Alzheimer’s disease (AD) research following the localization of ApoE on neurofibrillary tangles (NFT) and amyloids of senile plaques in the brains of AD patients [4]. Of the three alleles, the APOE ε4 (ε4) genotype is the greatest genetic risk factor

for AD as ε4 carriers of at least one allele are more than twice as likely as non-carriers to develop the disease, while the risk of AD in individuals expressing two ε4 alleles is 7-fold greater than non-carriers [5].

In the US, approximately two-thirds of patients afflicted with AD and other dementias over the age of 65 are women. The ε4 allele is: i) more often found in women with AD than men [6], ii) is associated with an earlier age of familial AD onset [7], and iii) presents an overall greater risk for developing AD [8]. Although these combined associated factors indicate that sex differences influence the pathogenesis and progression of AD, related studies investigating early cognitive decline in ε4 carriers have yielded contradicting findings. For instance, healthy men over the age of 65 that lack ε4 perform better in episodic recognition memory tasks than their ε4 counterparts while, in healthy women, the presence of ε4 does not affect performance [9]. In contrast, longitudinal studies show that ε4 women, but not men, have steeper declines and greater impairment in verbal memory and verbal learning [10]. The differences between male and female ε4 carriers suggest that APOE allelic variation differently alters the neural mechanisms that modulate learning and memory. The use of MRI to detect early differences in brain function prior to cognitive impairment may help in the early diagnosis of AD. To this point, asymptomatic male and female ε4 carriers ages 20–35 show increased connectivity across the default mode network (DMN) as compared to non-carrier controls [11].

In this study we utilized multiple imaging modalities in parallel with behavioral assays to identify sex-specific endophenotypes in an APOE-ε4 knock-in rat model (Horizon Discovery, Saint Louis, MO, USA). These findings were compared to imaging data from AD patients in the clinic. Surprisingly, the neuroradiological data indicates that ε4 females have fewer deficits in function and alterations in structure as compared to ε4 males.

Materials And Methods

Animals

Wild-type (WT) and human APOE ε4 knock-in (TGRA8960), male and female Sprague Dawley rats, (four groups, n = 6/group), were obtained from Horizon Discovery (Saint Louis MO). All rats were studied between four and five months of age. Rats were housed in Plexiglas cages (two per cage) and maintained in ambient temperature (22–24 °C) on a 12:12 light:dark cycle (lights on at 07:00 a.m.). Food and water were provided ad libitum. Rats were imaged during the light phase of the circadian cycle. All rats were acquired and cared for in accordance with the guidelines published in the NIH Guide for the Care and Use of Laboratory Animals. All methods and procedures described below were pre-approved by the Northeastern University Institutional Animal Care and Use Committee.

Transgenics

All animal work was performed in accordance with the approved animal protocols and Institutional Animal Care and Use Committee. Rats were housed in standard cages and maintained on a 12hr light/dark cycle with ad libitum access to food and water. Routine health monitoring of the colony was

performed at IDEXX (Columbia, MO) and revealed no evidence of infection with serious known pathogens.

Small guide RNA (sgRNA) template preparation

Two overlapping DNA oligonucleotides, one containing T7 promoter sequence and 20 nucleotides of Cas9 target sequence (specific oligo), and the other containing sgRNA backbone (common reverse oligo), were combined in a PCR reaction, together with a T7 forward and a backbone reverse primer. PCR was performed using AccuPrime HiFi Taq polymerase (Invitrogen, Waltham, MA USA) under the following conditions: 95^{o}C, 2 min, then 35 cycles of 95^{o}C, 30 sec; 60^{o}C, 30 sec; 68^{o}C, 30 sec. PCR product was purified by QiaQuick PCR purification kit (Qiagen, Venio, Netherlands), and the DNA was used as a template for in vitro sgRNA synthesis with HiScribe™ T7 Quick High Yield RNA Synthesis Kit (New England Biolabs, Whitby, ON, Canada). The RNA was purified by ethanol precipitation with 3M sodium acetate and quantified by Qubit BR RNA assay. Recombinant Cas9 protein was acquired from New England Biolabs.

Cas9 cleavage activity assay

Rat C6 glioma cells were maintained in F-12K media (ATCC) containing 15% horse serum, 2.5% FBS, and 1% penicillin/streptomycin at 37^{o}C with 5% CO2. All cell transfections were performed with a Nucleofector (Lonza, Basel, Switzerland) according to the manufacturer's 96-well shuttle protocol. Transfected cells were harvested 24 hours post-transfection into QuickExtract DNA extraction solution (Epicentre, Madison WI, USA), and incubated at 65^{o}C for 15 min and 98^{o}C for 3 min. Regions of interest were amplified by PCR using the extracted genomic DNA as a template and AccuStart II PCR SuperMix (Quanta Biosciences, Gaithersburg, MD, USA). The following PCR program was used: 95^{o}C, 2 min, 35 cycles of 95^{o}C, 15 sec, 60^{o}C, 15 sec, and 72^{o}C, 20 sec. Ten microliters of the above PCR reactions were incubated under the following program: 95^{o}C, 10 min, 95^{o}C to 85^{o}C, at -2^{o}C/s, 85^{o}C to 25^{o}C at -0.1^{o}C/s. One microliter each of nuclease S (Cel-I) and enhancer (Transgenomics, New Haven CT, USA) were added to digest the above reaction at 42^{o}C for 20 min. The mixture was resolved on a 10% polyacrylamide TBE gel.

Microinjection

Four- to five-week-old Sprague-Dawley female donors were injected with PMS followed by hCG injection after 48 hr of the PMS injection and then immediately mated with stud males after the hCG injection. Fertilized eggs were harvested a day later for microinjection. Microinjection reagents contained Cas9 protein/sgRNA (RNP) complex that was formed at 37^{o}C for five minutes, and then placed on ice until use. Just before a microinjection session, the RNP complex, donor plasmid, and injection buffer were carefully mixed together and injected into fertilized single-cell embryos. Injected zygotes were transferred into pseudo-pregnant females for live births.

Genotyping

Genotyping of live-born pups was performed by genomic PCR. Several reactions were routinely run to identify the founders that carried the desired mutation, such as 5' and 3' junctions, internal cassette, and plasmid backbone PCR to test for random integration of the DNA donor. Only founders positive by all PCR reactions and negative for plasmid backbone were verified by DNA sequencing.

Neuroimaging

Imaging sessions were conducted using a Bruker Biospec 7.0T/20-cm USR horizontal magnet (Bruker, Billerica, MA, USA) and a 20-G/cm magnetic field gradient insert (ID = 12 cm) capable of a 120-μs rise time. Radio frequency signals were sent and received with a quadrature volume coil built into the animal restrainer (Animal Imaging Research, Holden, Massachusetts). The design of the restraining system included a padded head support obviating the need for ear bars helping to reduce animal discomfort while minimizing motion artifact. All rats were imaged under 1% isoflurane with a respiratory rate of 40–50/min. At the beginning of each imaging session, a high-resolution anatomical data set was collected for volumetric analysis using the RARE pulse sequence with following parameters: TR/TE = 3310/36 ms; matrix size 256 × 256 × 40, field of view = 30 × 30 mm, spatial resolution, 0.117 × 0.117 × 0.7 mm.

Voxel-based morphometry analysis

A 3D MRI Rat Brain Atlas © (Ekam Solutions LLC, Boston, MA) was used to calculate brain volumes, and registered the standard structural rat template image onto high resolution T2-weighted images for each subject using a non-linear registration method implemented by Unix based software package Deformable Registration via Attribute Matching and Mutual-Saliency Weighting (DRAMMS; https://www.cbica.upenn.edu/sbia/software/dramms/index.html). The atlas (image size 256 × 256 × 63) (H x W x D) was then warped from the standard space into the subject image space (image size 256 × 256 × 40) using the deformation obtained from the above step using nearest-neighbor interpolation method. In the volumetric analysis, each brain region was therefore segmented, and the volume values were extracted for all 173 ROIs, calculated by multiplying unit volume of voxel in mm^3 by the number of voxels using an in-house MATLAB script. To account for different brain sizes, all ROI volumes were normalized by dividing each subject's ROI volume by their total brain volume

Diffusion weighted imaging – quantitative anisotropy

DWI was acquired with a spin-echo echo-planar-imaging (EPI) pulse sequence having the following parameters: TR/TE = 500/20 msec, eight EPI segments, and 10 non-collinear gradient directions with a single b-value shell at 1000s/mm^2 and one image with a B-value of 0 s/mm^2 (referred to as B_0). Geometrical parameters were: 48 coronal slices, each 0.313 mm thick (brain volume) and with in-plane resolution of 0.313 × 0.313 mm^2 (matrix size 96 × 96; FOV 30 mm^2). The imaging protocol was repeated two times for signal averaging. Each DWI acquisition took 35 min and the entire MRI protocol lasted ca. 70 min. Image analysis included DWI analysis of the DW-3D-EPI images to produce the maps of fractional anisotropy (FA) and apparent diffusion coefficient (ADC). DWI analysis was completed with MATLAB and MedINRIA (1.9.0; http://www-sop.inria.fr/asclepios/software/MedINRIA/index.php) software. Because sporadic excessive breathing during DWI acquisition can lead to significant image

motion artifacts that are apparent only in the slices sampled when motion occurred, each image (for each slice and each gradient direction) was screened, prior to DWI analysis. If found, acquisition points with motion artifacts were eliminated from analyses.

For statistical comparisons between rats, each brain volume was registered to the 3D rat atlas allowing voxel-based statistics. All image transformations and statistical analyses were carried out using the in-house MIVA software (http://ccni.wpi.edu/). For each rat, the B_0 image was co-registered with the B_0 template (using a 6-parameter rigid-body transformation). The co-registration parameters were then applied on the DWI indexed maps for the different indices of anisotropy. Normalization was performed on the maps since they provided the most detailed visualization of brain structures and allow for more accurate normalization. The normalization parameters were then applied to all DWI indexed maps that were then smoothed with a 0.3-mm Gaussian kernel. To ensure that FA and ADC values were not affected significantly by the pre-processing steps, the 'nearest neighbor' option was used following registration and normalization.

Statistical differences in measures of voxel-based morphology and DWI between genotypes and sex were determined using a nonparametric Newman-Keuls multiple comparisons test (alpha set at 5%) followed by post hoc analyses using a Wilcoxon rank-sum test for individual differences. The formula below was used to account for false discovery from multiple comparisons.

$$P_{(i)} \leq \frac{i}{V} \quad \frac{q}{c(V)}$$

P(i) is the p value based on the t test analysis. Each of 173 ROIs (i) within the brain containing (V) ROIs was ranked in order of its probability value (see Table 1). The false-positive filter value q was set to 0.2 and the predetermined c(V) was set to unity [12]. The corrected probability is noted on each table.

Resting state functional connectivity

Scans were collected using a spin-echo triple-shot EPI sequence (imaging parameters: matrix size = 96 × 96 × 20 (H x W x D), TR/TE = 1000/15 msec, voxel size = 0.312 × 0.312 × 1.2 mm, slice thickness = 1.2 mm, with 200 repetitions, time of acquisition 10 min. There are numerous studies detailing the benefits of multi-shot EPI in BOLD imaging [13–17]. We avoided using single shot EPI because of its sever geometrical distortion at high field strengths (≥ 7T) and loss of effective spatial resolution as the readout period increases [14, 18, 19]. There is also the possibility of signal loss in single shot EPI due to accumulated magnetic susceptibility or field inhomogeneity [13].

Preprocessing was accomplished through the use of the software packages: AFNI (NIHM, Rockville, MD), FSL (FMRIB, Oxford, UK), DRAMMS (SBIA, Philadelphia, PA) and MATLAB (Mathworks, Natick, MA). Brain tissue masks for resting-state functional images were manually drawn using 3DSlicer

(https://www.slicer.org/) and applied for skull-stripping. Motion outliers were detected in the dataset (i.e. data corrupted by extensive motion) and the corresponding time points were recorded so that they could be regressed out in a later step. Functional data were assessed for motion spikes, and large spikes were identified and removed in time-course signals, followed by slice timing correction from interleaved slice acquisition order. Head motion correction (six motion parameters) was carried out using the first volume as a reference image. Normalization was completed by registering functional data to the MRI rat brain atlas described above, using affine registration through DRAMMS. After quality assurance, band-pass filtering (0.01 Hz ~ 0.1 Hz) was preformed to reduce low-frequency drift effects and high-frequency physiological noise for each subject. The resulting images were further detrended and spatially smoothed (full width at half maximum [FWHM] = 0.8 mm). Finally, regressors comprised of motion outliers, the six motion parameters, the mean white matter (WM), and cerebrospinal fluid time series were fed into general linear models (GLM) for nuisance regression to remove unwanted effects.

The region-to-region functional connectivity method was performed to measure the correlations in spontaneous BOLD fluctuations. A network is comprised of nodes and edges; nodes being the ROIs and edges being the connections between regions. The 3D MRI Rat Brain Atlas containing 173 annotated brain regions was used for segmentation. Data are reported in 166 brain areas, as seven regions in the brain atlas were excluded from analysis due to the large size of three brains. These brains fell slightly outside our imaging field of view and thus we did not get any signal from the extreme caudal tip of the cerebellum and underlying brainstem. Whole brains that contain all regions of interest are needed for analyses so rather than excluding the animals, we removed the brain sites across all animals. Voxel time series data were averaged in each node based on the residual images using the nuisance regression procedure. Pearson's correlation coefficients across all pairs of nodes (13695 pairs) were computed for each subject among all three groups to assess the interregional temporal correlations. The correlation coefficients (ranging from − 1 to 1) were z-transformed using the Fisher's Z transform for normality. 166 × 166 symmetric connectivity matrices were constructed with each entry representing the strength of edge. Group-level analysis was performed to look at the functional connectivity in controls, and 4 rats. The resulting Z-score matrices from one-group t-tests were clustered using the K-nearest neighbors clustering method to identify how nodes cluster together and form resting state networks. An arbitrary Z-score threshold of |Z|=2.3 was applied to remove spurious or weak node connections.

Behavioral assay: novel object preference

A novel object preference test (NOP) was used to assess episodic learning and memory related stimulus recognition [20, 21]. The task was performed over the course of two days. On day one, rats were placed into a cube-shaped open field arena (100 cm x 100 cm x 35 cm black opaque plexiglass) for 15 minutes for habituation to the testing environment. The following day, for the first phase of testing (the familiar phase), rats were placed into the apparatus facing an unoccupied corner and allowed to investigate two identical objects (familiar objects) for 5 minutes, and then returned to their home cages for a 90-minute retention phase. After the retention phase, rats were again placed into the arena for an additional 3 minutes, this time with one of the familiar objects removed and replaced with a novel object. Objects for

both phases were placed in opposite corners, and were equidistant from each other and the perimeter of the field. Object presentation was counterbalanced for each rat, and the apparatus and objects were cleaned with 30% ethanol between each session to remove scent cues.

Behavioral assay: Barnes maze

The Barnes maze is used to assess spatial learning and memory for various rodent models [22–24]. The maze consists of a circular platform (diameter: 121 cm, elevated 40 cm), with 18 escape holes along the perimeter at 30 cm intervals. A black, removable enclosed Plexiglas “goal” box (l: 40.0 x w:12.7 x h:7.6 cm) was positioned under a single escape hole on the underside of the maze in the same position relative to the testing room across all trials. Between trials, the maze was rotated 45 degrees and the goal box was shifted accordingly for cardinal consistency.

Each trial began by placing an animal inside the goal box for 1 min and then under an enclosed container at the center of the maze for 30 sec. The container was then lifted to start the trial. For each trial, if the animals failed to reach the goal box within the test period (4 min), they were gently nudged into the goal box and allowed to stay for 1 min, and then placed back in their home cages between trials (3 trials/day for 4 days). All animals were analyzed for goal box latency (i.e., the amount of time before the animals entered the goal box), and path efficiency delta (i.e., the difference in path efficiency between acquisition days 1 and 4).

Behavioral assay: elevated plus maze

The Elevated Plus Maze (EPM) is a sensitive assay typically used to screen anxiolytic drug effects and is a valid apparatus for measuring anxious responding in rodents[25]. The apparatus consists of two open and two closed arms (l:30 x w:5 cm) arranged in a plus (“+”) shape elevated to a height of 38.5 cm with an intersecting in a central platform (l:5 x w:5 cm and black Plexiglas walls (15 cm high) lining the closed arms.

Animals were individually placed at the center of the apparatus facing one of the closed arms. The number of entries into the open arms, as well as the duration of time spent beyond a full body length in each arm were recorded for a period of 5 min for each animal. Increased entries and duration of time spent in the open arms is an established index of anxiolytic behavior, while the combine total number of entries into all arms of the maze provides a measure of locomotor activity.

Behavioral assays: statistics

For the NOP, each IR score group average was individually compared to chance (i.e., $\bar{x}$ = 50%) using a single-sample t-test, where an IR significantly greater than chance denotes preference for the novel object. For all behavioral assays, unless otherwise stated, groups were compared using 2-Way ANOVAs with planned comparison t-tests between 4 and their respective WT controls and then their respective sex counterparts (e.g., male 4 vs female 4, not male 4 vs female WT) to conserve power. For NOR, Barnes maze, and EPM all trials were digitally recorded. Data were analyzed using manual methods by

experimenters blind to treatment condition and verified with automated scoring using ANY-maze® software when possible (Stoelting, Wood Dale, IL).

Availability Of Data And Material

All data can be accessed through a link to Mandeley. DOI to follow

Results

Volumetric analysis

Shown in Fig. 1 are comparisons between WT females vs 4 females for differences in brain volumes (mm^3). The brain areas in the table are ranked in order of their significance and are truncated from a list of 173 areas. The 4 females have brain areas that are both larger and smaller than WT. The differences between female genotypes are summarized in the 3D color coded 3D representations to the right. The brain areas tend to cluster around larger brain regions like the sensorimotor ctx, hippocampal complex, cerebellum and brain stem. Several of the areas that are larger in 4 females are in the pons and brainstem (pontine reticular n., gigantocellularis reticular n., parvicellular reticular n. principle sensory n.) and are part of distributed neural circuitry of the reticular activating system. There were very few brain areas that differed in volume between the male genotypes (See Supplementary Fig. 1) Comparisons between WT females vs WT males and 4 females and 4 males were also few in number (See Supplementary Figs. 1 & 2).

Diffusion Weighted Imaging: Indices of Anisotropy

Shown in Fig. 2 are differences in FA values between WT females vs 4 females and WT males vs 4 males. A truncated table of 35 male brain areas ranked in order of their significance for FA values is shown (see Table 5S Supplementary Data for entire table). A comparable table for females lists only six significantly different areas (see Table 6S Supplementary Data for entire table) the identity of which are shown in the 2D probability maps and are primarily associated with the olfactory bulb and ventral striatum (accumbens, ventral pallidum). In all cases, 4 males have higher FA values than WT males primarily associated with the sensorimotor and limbic cortices and the primary olfactory system (bulb, tenia tecta, anterior olfactory n.). The same pattern exists when comparing 4 females to 4 males with males showing 34 brain areas that have significantly higher FA in olfactory system, sensorimotor ctx and brainstem nuclei (Table 7S Supplementary Data). There were 45 brain areas with differences in FA values between WT females vs WT males (Table 8S Supplementary Data). Values were higher in 29/45 areas for females that included much of the basal ganglia, ventral striatum and midbrain dopaminergic system.

Shown in Fig. 3 are differences in ADC values between WT females vs 4 females and WT males vs 4 males. Truncated tables of 26 male brain areas and 14 female brain areas ranked in order of their significance for ADC values are shown (see Table 9S & 10S Supplementary Data for entire tables). In all

areas shown male 4 rats show greater ADC values than male WT. The differences are primarily confined to hindbrain areas, cerebellum and brainstem reticular activating system as shown in the 2D probability maps and 3D reconstructions. In contrast, in all cases but one (medial mammillary n.) female WT rats show higher ADC values than their 4 counterparts. These differences included the ventral hippocampus and much of the cerebellum. Approximately 50% of all brain regions differed in ADC values between 4 females and 4 males with values in males being higher than females (Table 11S Supplementary Data). There are 48 brain areas that differ in ADC values when comparing WT females vs WT males with a majority being higher in males (Table 12S Supplementary Data).

Resting State Functional Connectivity

Shown in Fig. 4 are correlation matrices between 166 brain areas for resting state functional connectivity (rsFC) between for male and female genotypes. The diagonal line separates the two sex specific genotypes. The brain areas with significant correlations often appear as clusters because they are contiguous in their neuroanatomy and function. The marked areas labeled in the correlation matrices highlight the differences between genotypes. These differences are absent or not as obvious between the male genotypes. Graph analysis identified four brain areas or nodes in the 4 female genotype that had significant connections with and between other brain areas as shown in Fig. 5. These areas include the midbrain linear n. of the raphe, reuniens nucleus of the thalamus, paraventricular n. of the hypothalamus and the midbrain reticular n. Each of the rows show significant Z values for brain areas between and with each node. These integrated brain areas cluster around the amygdala, hypothalamus, hippocampus, ventral striatum, and midbrain/pontine reticular activating system. These integrated brain areas are color coded and shown in 3D in the glass brain together with their connections to the four key nodes. Note how the key nodes align along the midline axial, the nodes align along the midline rostral caudal axis.

Behavioral Assays

Figure 6 is a composite of data from both sexes and genotypes showing Barnes maze and Novel Object Preference performance. Barnes testing yielded a significant main effect of genotype ($F_{(1,30)} = 8.4$, $P < 0.01$) with both male and female 4 rats showing longer goal latencies in comparison to their WT counterparts (females: $t(22) = 2.17$, $P < 0.05$; males: $t(8) = 2.05$, $P < 0.05$). When broken down by acquisition day, there were main effects of both genotype ($F_{(3,30)} = 3.08$, $P < 0.05$) and days ($F_{(3,90)} = 11.6$, $P < 0.0001$) for goal box latency, with planned comparisons revealing a significant difference between 4 and WT females on the first day of acquisition ($t(22) = 2.90$, $P < 0.05$), with an additional marginally significant difference between 4 males and 4 females on day 2 ($t(15) = 1.90$, $P = 0.06$). As an index of learning, we also examined the change in path efficiency from acquisition day 1 to day 4 (path efficiency delta) and found a significant interaction across groups ($F_{(3,30)} = 4.58$, $P < 0.05$) driven by a difference between 4 males and 4 females ($t(15) = 3.31$, $P < 0.01$) where 4 males became less efficient at finding the goal box, while 4 females became more efficient over acquisition days.

For NOP testing, all but ε4 males spent more time exploring the novel object beyond chance levels ($\bar{x}$ = 50% of the total testing time) as measured by one-sample t-tests (WT females: $t(11) = 2.68$, $p < 0.05$; ε4 females: $t(11) = 3.73$, $p < 0.01$; WT males: $t(4) = 19.28$, $p < 0.0001$; ε4 males: $t(4) = 0.69$, $p > 0.05$). When the total time spent exploring the novel object was compared between groups, there was a significant interaction ($F_{(1,30)} = 7.34$, $P < 0.05$) driven by a significant difference between WT and ε4 males ($t(8) = 2.87$, $P < 0.01$) and a marginal difference between ε4 males and ε4 females ($t(15) = 1.99$, $P = 0.06$).

Elevated plus maze testing showed a main effect of genotype ($F_{(1,30)} = 5.63$, $P < 0.05$), with male ε4 males showing more anxiety-like behavior (i.e., spent less time on the open arm) than their wildtype counterparts ($t(8) = 2.08$, $P < 0.05$; see Fig. 7).

Discussion

The purpose of this study was to use MRI to characterize the neuroanatomical, and functional differences between transfected male and female rats homozygous for the human APOE ε4 allele at 6 months of age. The imaging protocols are the same used in the clinic helping in the translation of these finding to the human condition. In the clinic, differences in disease onset and severity between female and male ε4 carriers have been well described [26, 27] with women carriers having a greater risk for AD then men [8, 28–30]. Given these clinical findings we hypothesized that female ε4 rats would present with cognitive deficits and alterations in global brain structure, function, and hippocampal neurocircuitry similar to that of patients with early onset familial AD. The data however, fell contrary to our expectation. The behavioral analyses indicate that only male ε4 rats have impaired stimulus preference and object memory at this age. Female ε4 had larger brain volumes in reticular activating system (RAS), brainstem, and cerebellum than WT females, while there were no significant differences in brain volumes between male genotypes. Putative changes in gray matter microarchitecture ascertained from DWI were more common in male ε4 carriers than female carriers. Male ε4 rats showed extensive increases in FA and ADC across the cerebellar region, brainstem, and cortex. Resting state brain activity showed greater connectivity in female carriers as compared to males. The discussion that follows compares these neuroimaging data to those collected in the clinic, providing potential evidence of early neuroradiological signs of pathology in ε4 genotypes.

Voxel Based Morphometry

In the case of voxel and ROI based volumetric analysis, the data from elderly human ε4 carriers with normal cognition are equivocal as whole brain and hippocampal gray matter volume are unchanged [31–33], decreased [34], and even increased [35]. The translational value of volumetric analyses was not obvious from our studies, as male ε4 rats showed very few differences in brain area volumes as compared to WT controls, while female ε4 rats showed site-specific increases and decreases across many regions.

Diffusion Weighted Imaging with Quantitative Anisotropy

While there are many studies on diffusion tensor imaging with indices of anisotropy that characterize white matter fiber tracts in ε4 carriers [36–39], we are not aware of any study (animal or human) using diffusion weighted imaging to follow changes in gray matter microarchitecture over the entire brain of the ε4 genotype. One study comparing AD patients (genotype unknown) to normal controls reported increased ADC values for the hippocampus, and suggested that this increase in water diffusion may reflect a change in gray matter microarchitecture associated with progression of AD [40]. More recently, it was reported that AD patients present with an increase in ADC in the precuneus ctx [41], an area involved in mental imagery and episodic memory[42]. The ADC values in our male ε4 rats were greater than their WT controls, but these increases were located primarily in the brainstem, cerebellum, and entorhinal ctx; a key area in the hippocampal circuitry. Compared to WT controls, female ε4 rats showed a significant decrease in ADC values in both the entorhinal ctx and ventral hippocampus. This sex-dependent inverse relationship in entorhinal ADC values in ε4 carriers may have some translational value and signal the early stages of disease progression in males. While only speculative, the enhanced ADC in male ε4 could reflect an increase in the extracellular fluid volume possibly caused by small vessel disease with vasogenic edema. Cerebral amyloid angiopathy involves the deposition of amyloid β in the walls of arterioles and capillaries[43, 44]. Interestingly, the insinuation of amyloid β into the wall of capillaries is associated with APOEε4 [43, 44].

Compared to WT controls, ε4 rats showed evidence of altered gray matter microarchitecture with measures of diffusivity. Changes in measures of diffusivity were most prevalent in males. Of particular note, the deep cerebellar nuclei, as well as various hindbrain regions including the locus coeruleus (LC), showed increased FA values. These alterations correspond to recent human studies that suggest that the neuropathogenesis of AD may begin well before the onset of clinical signs of AD specifically within hindbrain regions, and most notably within the raphe and LC. Indeed, these areas show early accumulation of neurofibrillary tangles and neuronal loss with AD pathogenesis [45–48]. The LC receives input from the deep cerebellar nuclei and projects back to the cerebellar region in close proximity to, or within, the fastigial and interposed nuclei [49, 50]. These connections are important since, although cerebellum function has historically been aligned with fine motor coordination, there are numerous reports of cerebellar regulation of autonomic physiology [51–53], emotion, and cognition [52, 54, 55]. Despite the fact we only recorded limited differences in motor behavior between male genotypes, it is possible that the altered FA in the LC, deep cerebellar nuclei, and cerebellum represent anatomical predicates to behavioral deficits that will worsen with aging.

Resting State Functional Connectivity

Reduced connectivity within the default mode network (DMN) that connects the medial prefrontal ctx with the anterior/posterior cingulate, precuneus, parietal, and temporal cortices, is a putative biomarker of AD [56–59], and occurs early in the progression of various forms of the disease[60] [57, 61]. Interestingly, asymptomatic male and female ε4 carriers ages 20–35 show increased connectivity across the anterior/posterior DMN as compared to controls [11]. Similarly, older, cognitively normal ε4 carriers also present with an increase in connectivity with the DMN, and between the DMN and salience network (SN)

that comprises the insular and anterior cingulate cortices and their connections to ventral striatum, midbrain dopaminergic system, amygdala, and hypothalamus [11, 62–66]. The hyperconnectivity we observed in female ε4 rats is analogous to the increased connectivity in the human SN as the ventral striatum, amygdala, and hypothalamus are synchronized together with the RAS.

The DMN and SN show anti-correlation such that when one is active the other is silent. This relationship along with balanced activity between the DMN and SN led Machulda and workers [65] to propose that increased connectivity in ε4 carriers, particularly in the SN, is due to a loss of inhibitory control from the DMN. This proposal is contrary to the prevailing hypothesis that hyperconnectivity compensates for a decline in cognitive function [67]. In our study, we did not see any anti-correlation using transgenic rats. Regardless, increased connectivity comes with a metabolic cost and the affected neural circuitry may be at risk with aging [64, 68].

Functional connectivity data showed a clear sex difference in ε4 carriers (see Fig. 4). Male ε4 rats were no different from their WT controls. In contrast, female ε4 carriers showed hyperconnectivity across multiple brain areas particularly in the amygdala, RAS, hypothalamus, and raphe/forebrain circuitry. From these four brain regions came four interconnected key nodes that aligned along the basal midline extending from the hypothalamus to brainstem (Fig. 5). The caudal most node, the linear raphe nucleus, is considered part of the RAS, controlling emotion reactivity through serotonergic signaling [69]. The reuniens nucleus is the major thalamic input to the hippocampus and is critical for memory retrieval and spatial working memory [70, 71]. The reuniens is also involved in cognition and executive function by forming a link between the prefrontal cortex and the hippocampus [72]. The paraventricular nucleus (PVN) (one of the four key nodes identified in Fig. 5) plays a seminal role in the hypothalamic neuroendocrine system and the maintenance of homeostasis. Interestingly, the PVN receives inputs from the reuniens [73]. The reticular n. of the midbrain is part of the ascending RAS with extensive connections to hypothalamus, thalamus, and basal forebrain involved in spatial attention and arousal [74].

Translational animal models: rat versus mouse

The behavioral phenotypes differ between ε4 rats and ε4 mice. In our studies, male ε4 rats showed a modest decrease in cognitive ability while ε4 females showed no change. These results conflict with several studies in human ε4 mouse models. For example, female but not male ε4 mice show deficits in social and spatial memory as early as 4–6 months[75, 76] [77, 78]). Only at 11–14 months do male ε4 mice begin to display evidence of poor working memory [79] suggesting female ε4 mice may be vulnerable across a larger portion of their lifetime to learning and memory deficits compared to males. These data contrast our studies that show that female ε4 rats show no cognitive deficits as late as 6 months of age while males show signs of impairment.

Multimodal imaging data from male ε4 mice at 12–18 months indicate that cerebral blood flow to the cortex and hippocampus is reduced, and that rsFC is attenuated across the cortical mantel, and between the ctx and hippocampus [80, 81]. DWI data from mice indicate an increase in diffusivity in the cortex and hippocampus can occur at 18 months of age, along with decreases in FA in the hippocampus and

piriform ctx [80]. Male ε4 mice studied at 24 months of age showed atrophy in the cortex and hippocampus as compared to WT controls [82]. At six months of age, the male ε4 rats used in our study showed no change in rsFC compared to WT, but extensive changes in ADC and FA values primarily in the brainstem, cerebellum, olfactory system, and cortex. Brain volumes at six months of age were similar to WT. There are no other MRI studies that we are aware of using female ε4 rodents. In these studies, the changes between WT and ε4 females are very significant for brain volumes and rsFC. While these studies were at six months of age and not 1–2 years as reported in mice, female ε4 rats showed enhanced connectivity compared to WT.

Limitations

There are several limitations that should be noted. 1) It is not possible to draw any conclusions about the pleiotropic effects of the ε4 isoform without longitudinal data covering the natural life-span of the rat. 2) These studies would have benefited from immunohistochemical data for oxidative stress, mitochondrial dysfunction, neuroinflammation, or biomarkers of AD to assess the level of disease progression. 3) The rsFC data were collected under low dose isoflurane anesthesia to minimize motion artifact and physiological stress [83]. Nonetheless, numerous studies comparing anesthetized and conscious states show similar rsFC data [84, 85]. However, the absence of anti-correlation data in these studies may be attributable to the use of anesthesia [86].

Speculation - antagonistic pleiotropy

Several studies have reported the beneficial effects that the ε4 allele may have for young carriers. A condition that has detrimental consequences with aging but positive effects during development is referred to as antagonistic pleiotropy [87]. In the context of AD, antagonistic pleiotropy was originally posited by Alexander and coworkers when they reported enhanced semantic and phonetic fluency in a proband of ε4 subjects ranging from 6 to 65 years of age [88]. Accordingly, there have been several reports showing young carriers outperform peers on numerous tests of learning and memory [89–91]. This advantage may be related to differences in carrier neuroanatomy and physiology since young ε4 carriers present with a larger gray matter volume [92], increased cerebral blood flow [93], and enhanced functional connectivity [11, 62–66]. The integrated nodes in the female ε4 rat discussed above would suggest a behavioral phenotype open to better learning and memory on a background of increased vigilance not unlike young human ε4 carriers.

The frequency of ε4 allele is highest in non-industrialized populations in equatorial and tropical areas[94]. In rural Ghana and Ecuador, ε4 carriers show a significant gene effect for increased fertility and survival of offspring in the face of a high infectious load [95, 96]. It is hypothesized that the ε4 isoform provides high levels of cholesterol precursor to ovaries for progesterone and estrogen synthesis for enhanced reproductive fertility [97]. Plasma samples from ε4 carriers inhibit growth of the parasite Plasmodium falciparum [98] and may confer some resistance to malaria [99, 100]. In a rural Amazon population with a high parasitic load, ε4 carriers demonstrate better cognitive ability than non-carriers across the life span demonstrating a gene-by-environment interaction that has a selective advantage under pathogenic

conditions [101]. This advantage is evident in both men and women, across all ages, and thus, antagonistic pleiotropy may not be the rule in preindustrial, rural populations with high levels of infection. As such, the selective advantage may be lost in industrialized populations with access to sanitation resources and clean water.

Conclusion

In these studies, using six-month old female and male ε4 rats, there is a clear sex difference between ε4 carriers which is most obvious in measures of functional connectivity. The functional connectivity was centered around four key nodes aligned along the midline extending from the hypothalamus to the midbrain that integrated emotion, motivation, and memory with the reticular activating system. Hyperconnectivity across these areas is analogous to the enhanced connectivity in the human SN circuit in asymptomatic ε4 carriers. In many respects, these female ε4 rats reflect young asymptomatic human ε4 carriers. While only speculative, the collective behavioral and neuroradiological data would suggest that female ε4 rats, at this age, have a selective advantage over non-carriers. However, the hyperconnectivity comes with a metabolic cost, and the same integrated circuit may be vulnerable to redox stress and mitochondrial dysfunction with aging. This scenario would fit the description of female-specific antagonistic pleiotropy. Why young female ε4 mice show the opposite effect is uncertain. Perhaps the extreme sanitation of commercial breeders has some part to play. Would a feral mouse or rat with the human APOEε4 be a better model?

Declarations

Ethics approval and consent to participate

Not applicable

Consent for publication

Yes

Availability of data and material

All data can be accessed through a link to Mandeley. DOI to follow

Competing interests

CFF has a financial interest in Animal Imaging Research, the company that makes the RF electronics and holders for animal imaging

Funding

None

Authors' contributions

All of the authors have contributed substantially to the manuscript.

Conception and Design CFF, PK, TM, SG; Acquisition and Analysis PK, CFF, XC, SG, MT, JH, HB, JCH, SI; Drafting of Manuscript CFF, DM, TM, BCK

Acknowledgements

We owe a debt of gratitude to Mark Nedelman, Biomere in the support of this research.

References

1. Mahley RW: **Apolipoprotein E: cholesterol transport protein with expanding role in cell biology**. *Science* 1988, **240**(4852):622-630.
2. Hauser PS, Narayanaswami V, Ryan RO: **Apolipoprotein E: from lipid transport to neurobiology**. *Progress in lipid research* 2011, **50**(1):62-74.
3. Weisgraber KH, Rall SC, Jr., Mahley RW: **Human E apoprotein heterogeneity. Cysteine-arginine interchanges in the amino acid sequence of the apo-E isoforms**. *J Biol Chem* 1981, **256**(17):9077-9083.
4. Namba Y, Tomonaga M, Kawasaki H, Otomo E, Ikeda K: **Apolipoprotein E immunoreactivity in cerebral amyloid deposits and neurofibrillary tangles in Alzheimer's disease and kuru plaque amyloid in Creutzfeldt-Jakob disease**. *Brain Res* 1991, **541**(1):163-166.
5. Kuusisto J, Koivisto K, Kervinen K, Mykkanen L, Helkala EL, Vanhanen M, Hanninen T, Pyorala K, Kesaniemi YA, Riekkinen P *et al*: **Association of apolipoprotein E phenotypes with late onset Alzheimer's disease: population based study**. *BMJ* 1994, **309**(6955):636-638.
6. Poirier J, Davignon J, Bouthillier D, Kogan S, Bertrand P, Gauthier S: **Apolipoprotein E polymorphism and Alzheimer's disease**. *Lancet* 1993, **342**(8873):697-699.
7. Duara R, Barker WW, Lopez-Alberola R, Loewenstein DA, Grau LB, Gilchrist D, Sevush S, St George-Hyslop S: **Alzheimer's disease: interaction of apolipoprotein E genotype, family history of dementia, gender, education, ethnicity, and age of onset**. *Neurology* 1996, **46**(6):1575-1579.
8. Altmann A, Tian L, Henderson VW, Greicius MD, Alzheimer's Disease Neuroimaging Initiative I: **Sex modifies the APOE-related risk of developing Alzheimer disease**. *Ann Neurol* 2014, **75**(4):563-573.
9. Sundermann EE, Gilbert PE, Murphy C: **Apolipoprotein E epsilon4 genotype and gender: effects on memory**. *Am J Geriatr Psychiatry* 2007, **15**(10):869-878.
10. Beydoun MA, Boueiz A, Abougergi MS, Kitner-Triolo MH, Beydoun HA, Resnick SM, O'Brien R, Zonderman AB: **Sex differences in the association of the apolipoprotein E epsilon 4 allele with incidence of dementia, cognitive impairment, and decline**. *Neurobiol Aging* 2012, **33**(4):720-731 e724.

11. Filippini N, MacIntosh BJ, Hough MG, Goodwin GM, Frisoni GB, Smith SM, Matthews PM, Beckmann CF, Mackay CE: **Distinct patterns of brain activity in young carriers of the APOE-epsilon4 allele**. *Proc Natl Acad Sci U S A* 2009, **106**(17):7209-7214.
12. Benjamini Y, Hochberg Y: **Controlling the false discovery rate: A practical and powerful approach to multiple testing**. *Journal of the Royal Statistical Society Series B (Methodological)* 1995, **57**(1):289-300.
13. Kang D, Sung YW, Kang CK: **Fast Imaging Technique for fMRI: Consecutive Multishot Echo Planar Imaging Accelerated with GRAPPA Technique**. *BioMed research international* 2015, **2015**:394213.
14. Hoogenraad FG, Pouwels PJ, Hofman MB, Rombouts SA, Lavini C, Leach MO, Haacke EM: **High-resolution segmented EPI in a motor task fMRI study**. *Magn Reson Imaging* 2000, **18**(4):405-409.
15. Swisher JD, Sexton JA, Gatenby JC, Gore JC, Tong F: **Multishot versus single-shot pulse sequences in very high field fMRI: a comparison using retinotopic mapping**. *PLoS One* 2012, **7**(4):e34626.
16. Menon RS, Thomas CG, Gati JS: **Investigation of BOLD contrast in fMRI using multi-shot EPI**. *NMR in biomedicine* 1997, **10**(4-5):179-182.
17. Poser BA, Norris DG: **Investigating the benefits of multi-echo EPI for fMRI at 7 T**. *NeuroImage* 2009, **45**(4):1162-1172.
18. Farzaneh F, Riederer SJ, Pelc NJ: **Analysis of T2 limitations and off-resonance effects on spatial resolution and artifacts in echo-planar imaging**. *Magn Reson Med* 1990, **14**(1):123-139.
19. Jesmanowicz A, Bandettini PA, Hyde JS: **Single-shot half k-space high-resolution gradient-recalled EPI for fMRI at 3 Tesla**. *Magn Reson Med* 1998, **40**(5):754-762.
20. Antunes M, Biala G: **The novel object recognition memory: neurobiology, test procedure, and its modifications**. *Cogn Process* 2012, **13**(2):93-110.
21. Bevins RA, Besheer J: **Object recognition in rats and mice: a one-trial non-matching-to-sample learning task to study 'recognition memory'**. *Nature protocols* 2006, **1**(3):1306-1311.
22. Barnes CA: **Memory deficits associated with senescence: a neurophysiological and behavioral study in the rat**. *J Comp Physiol Psychol* 1979, **93**(1):74-104.
23. Fox GB, Fan L, LeVasseur RA, Faden AI: **Effect of traumatic brain injury on mouse spatial and nonspatial learning in the Barnes circular maze**. *Journal of neurotrauma* 1998, **15**(12):1037-1046.
24. Harrison FE, Hosseini AH, McDonald MP: **Endogenous anxiety and stress responses in water maze and Barnes maze spatial memory tasks**. *Behav Brain Res* 2009, **198**(1):247-251.
25. Carobrez AP, Bertoglio LJ: **Ethological and temporal analyses of anxiety-like behavior: the elevated plus-maze model 20 years on**. *Neurosci Biobehav Rev* 2005, **29**(8):1193-1205.
26. Mosconi L, Berti V, Quinn C, McHugh P, Petrongolo G, Varsavsky I, Osorio RS, Pupi A, Vallabhajosula S, Isaacson RS *et al*: **Sex differences in Alzheimer risk: Brain imaging of endocrine vs chronologic aging**. *Neurology* 2017, **89**(13):1382-1390.
27. Sohn D, Shpanskaya K, Lucas JE, Petrella JR, Saykin AJ, Tanzi RE, Samatova NF, Doraiswamy PM: **Sex Differences in Cognitive Decline in Subjects with High Likelihood of Mild Cognitive Impairment**

due to Alzheimer's disease. *Scientific reports* 2018, **8**(1):7490.

28. Fleisher A, Grundman M, Jack CR, Jr., Petersen RC, Taylor C, Kim HT, Schiller DH, Bagwell V, Sencakova D, Weiner MF *et al*: **Sex, apolipoprotein E epsilon 4 status, and hippocampal volume in mild cognitive impairment**. *Arch Neurol* 2005, **62**(6):953-957.
29. Bretsky PM, Buckwalter JG, Seeman TE, Miller CA, Poirier J, Schellenberg GD, Finch CE, Henderson VW: **Evidence for an interaction between apolipoprotein E genotype, gender, and Alzheimer disease**. *Alzheimer Dis Assoc Disord* 1999, **13**(4):216-221.
30. Holland D, Desikan RS, Dale AM, McEvoy LK, Alzheimer's Disease Neuroimaging I: **Higher rates of decline for women and apolipoprotein E epsilon4 carriers**. *AJNR American journal of neuroradiology* 2013, **34**(12):2287-2293.
31. Protas HD, Chen K, Langbaum JB, Fleisher AS, Alexander GE, Lee W, Bandy D, de Leon MJ, Mosconi L, Buckley S *et al*: **Posterior cingulate glucose metabolism, hippocampal glucose metabolism, and hippocampal volume in cognitively normal, late-middle-aged persons at 3 levels of genetic risk for Alzheimer disease**. *JAMA neurology* 2013, **70**(3):320-325.
32. Hostage CA, Roy Choudhury K, Doraiswamy PM, Petrella JR, Alzheimer's Disease Neuroimaging I: **Dissecting the gene dose-effects of the APOE epsilon4 and epsilon2 alleles on hippocampal volumes in aging and Alzheimer's disease**. *PLoS One* 2013, **8**(2):e54483.
33. Bunce D, Anstey KJ, Cherbuin N, Gautam P, Sachdev P, Easteal S: **APOE genotype and entorhinal cortex volume in non-demented community-dwelling adults in midlife and early old age**. *Journal of Alzheimer's disease : JAD* 2012, **30**(4):935-942.
34. Chen K, Reiman EM, Alexander GE, Caselli RJ, Gerkin R, Bandy D, Domb A, Osborne D, Fox N, Crum WR *et al*: **Correlations between apolipoprotein E epsilon4 gene dose and whole brain atrophy rates**. *Am J Psychiatry* 2007, **164**(6):916-921.
35. Striepens N, Scheef L, Wind A, Meiberth D, Popp J, Spottke A, Kolsch H, Wagner M, Jessen F: **Interaction effects of subjective memory impairment and ApoE4 genotype on episodic memory and hippocampal volume**. *Psychological medicine* 2011, **41**(9):1997-2006.
36. Nierenberg J, Pomara N, Hoptman MJ, Sidtis JJ, Ardekani BA, Lim KO: **Abnormal white matter integrity in healthy apolipoprotein E epsilon4 carriers**. *Neuroreport* 2005, **16**(12):1369-1372.
37. Persson J, Lind J, Larsson A, Ingvar M, Cruts M, Van Broeckhoven C, Adolfsson R, Nilsson LG, Nyberg L: **Altered brain white matter integrity in healthy carriers of the APOE epsilon4 allele: a risk for AD?** *Neurology* 2006, **66**(7):1029-1033.
38. Westlye LT, Reinvang I, Rootwelt H, Espeseth T: **Effects of APOE on brain white matter microstructure in healthy adults**. *Neurology* 2012, **79**(19):1961-1969.
39. Operto G, Cacciaglia R, Grau-Rivera O, Falcon C, Brugulat-Serrat A, Rodenas P, Ramos R, Moran S, Esteller M, Bargallo N *et al*: **White matter microstructure is altered in cognitively normal middle-aged APOE-epsilon4 homozygotes**. *Alzheimer's research & therapy* 2018, **10**(1):48.
40. Kantarci K, Jack CR, Jr., Xu YC, Campeau NG, O'Brien PC, Smith GE, Ivnik RJ, Boeve BF, Kokmen E, Tangalos EG *et al*: **Mild cognitive impairment and Alzheimer disease: regional diffusivity of water**.

Radiology 2001, **219**(1):101-107.

41. Takahashi H, Ishii K, Kashiwagi N, Watanabe Y, Tanaka H, Murakami T, Tomiyama N: **Clinical application of apparent diffusion coefficient mapping in voxel-based morphometry in the diagnosis of Alzheimer's disease**. *Clinical radiology* 2017, **72**(2):108-115.
42. Fletcher PC, Frith CD, Baker SC, Shallice T, Frackowiak RS, Dolan RJ: **The mind's eye--precuneus activation in memory-related imagery**. *NeuroImage* 1995, **2**(3):195-200.
43. Charidimou A, Gang Q, Werring DJ: **Sporadic cerebral amyloid angiopathy revisited: recent insights into pathophysiology and clinical spectrum**. *Journal of neurology, neurosurgery, and psychiatry* 2012, **83**(2):124-137.
44. Yamada M: **Cerebral amyloid angiopathy: emerging concepts**. *Journal of stroke* 2015, **17**(1):17-30.
45. Braak H, Del Tredici K: **The pathological process underlying Alzheimer's disease in individuals under thirty**. *Acta neuropathologica* 2011, **121**(2):171-181.
46. Rub U, Del Tredici K, Schultz C, Thal DR, Braak E, Braak H: **The evolution of Alzheimer's disease-related cytoskeletal pathology in the human raphe nuclei**. *Neuropathology and applied neurobiology* 2000, **26**(6):553-567.
47. Theofilas P, Ehrenberg AJ, Dunlop S, Di Lorenzo Alho AT, Nguy A, Leite REP, Rodriguez RD, Mejia MB, Suemoto CK, Ferretti-Rebustini REL *et al*: **Locus coeruleus volume and cell population changes during Alzheimer's disease progression: A stereological study in human postmortem brains with potential implication for early-stage biomarker discovery**. *Alzheimers Dement* 2017, **13**(3):236-246.
48. Theofilas P, Ehrenberg AJ, Nguy A, Thackrey JM, Dunlop S, Mejia MB, Alho AT, Paraizo Leite RE, Rodriguez RD, Suemoto CK *et al*: **Probing the correlation of neuronal loss, neurofibrillary tangles, and cell death markers across the Alzheimer's disease Braak stages: a quantitative study in humans**. *Neurobiol Aging* 2018, **61**:1-12.
49. Clavier RM: **Afferent projections to the self-stimulation regions of the dorsal pons, including the locus coeruleus, in the rat as demonstrated by the horseradish peroxidase technique**. *Brain Res Bull* 1979, **4**(4):497-504.
50. Cedarbaum JM, Aghajanian GK: **Afferent projections to the rat locus coeruleus as determined by a retrograde tracing technique**. *J Comp Neurol* 1978, **178**(1):1-16.
51. Snider RS, Maiti A: **Cerebellar contributions to the Papez circuit**. *Journal of neuroscience research* 1976, **2**(2):133-146.
52. Haines DE, Dietrichs E, Sowa TE: **Hypothalamo-cerebellar and cerebello-hypothalamic pathways: a review and hypothesis concerning cerebellar circuits which may influence autonomic centers affective behavior**. *Brain, behavior and evolution* 1984, **24**(4):198-220.
53. Cavdar S, San T, Aker R, Sehirli U, Onat F: **Cerebellar connections to the dorsomedial and posterior nuclei of the hypothalamus in the rat**. *Journal of anatomy* 2001, **198**(Pt 1):37-45.
54. Newman PP, Paul DH: **The projection of splanchnic afferents on the cerebellum of the cat**. *J Physiol* 1969, **202**(1):223-227.

55. Perciavalle V, Apps R, Bracha V, Delgado-Garcia JM, Gibson AR, Leggio M, Carrel AJ, Cerminara N, Coco M, Gruart A *et al*: **Consensus paper: current views on the role of cerebellar interpositus nucleus in movement control and emotion**. *Cerebellum* 2013, **12**(5):738-757.
56. Balthazar ML, de Campos BM, Franco AR, Damasceno BP, Cendes F: **Whole cortical and default mode network mean functional connectivity as potential biomarkers for mild Alzheimer's disease**. *Psychiatry research* 2014, **221**(1):37-42.
57. Greicius MD, Srivastava G, Reiss AL, Menon V: **Default-mode network activity distinguishes Alzheimer's disease from healthy aging: evidence from functional MRI**. *Proc Natl Acad Sci U S A* 2004, **101**(13):4637-4642.
58. Jones DT, Machulda MM, Vemuri P, McDade EM, Zeng G, Senjem ML, Gunter JL, Przybelski SA, Avula RT, Knopman DS *et al*: **Age-related changes in the default mode network are more advanced in Alzheimer disease**. *Neurology* 2011, **77**(16):1524-1531.
59. Hohenfeld C, Werner CJ, Reetz K: **Resting-state connectivity in neurodegenerative disorders: Is there potential for an imaging biomarker?** *NeuroImage Clinical* 2018, **18**:849-870.
60. Chhatwal JP, Schultz AP, Johnson K, Benzinger TL, Jack C, Jr., Ances BM, Sullivan CA, Salloway SP, Ringman JM, Koeppe RA *et al*: **Impaired default network functional connectivity in autosomal dominant Alzheimer disease**. *Neurology* 2013, **81**(8):736-744.
61. Celone KA, Calhoun VD, Dickerson BC, Atri A, Chua EF, Miller SL, DePeau K, Rentz DM, Selkoe DJ, Blacker D *et al*: **Alterations in memory networks in mild cognitive impairment and Alzheimer's disease: an independent component analysis**. *J Neurosci* 2006, **26**(40):10222-10231.
62. Fleisher AS, Sherzai A, Taylor C, Langbaum JB, Chen K, Buxton RB: **Resting-state BOLD networks versus task-associated functional MRI for distinguishing Alzheimer's disease risk groups**. *NeuroImage* 2009, **47**(4):1678-1690.
63. Sheline YI, Morris JC, Snyder AZ, Price JL, Yan Z, D'Angelo G, Liu C, Dixit S, Benzinger T, Fagan A *et al*: **APOE4 allele disrupts resting state fMRI connectivity in the absence of amyloid plaques or decreased CSF Abeta42**. *J Neurosci* 2010, **30**(50):17035-17040.
64. Westlye ET, Lundervold A, Rootwelt H, Lundervold AJ, Westlye LT: **Increased hippocampal default mode synchronization during rest in middle-aged and elderly APOE epsilon4 carriers: relationships with memory performance**. *J Neurosci* 2011, **31**(21):7775-7783.
65. Machulda MM, Jones DT, Vemuri P, McDade E, Avula R, Przybelski S, Boeve BF, Knopman DS, Petersen RC, Jack CR, Jr.: **Effect of APOE epsilon4 status on intrinsic network connectivity in cognitively normal elderly subjects**. *Arch Neurol* 2011, **68**(9):1131-1136.
66. Ye Q, Chen H, Su F, Shu H, Gong L, Xie C, Zhou H, Bai F: **An Inverse U-Shaped Curve of Resting-State Networks in Individuals at High Risk of Alzheimer's Disease**. *The Journal of clinical psychiatry* 2018, **79**(2).
67. Han SD, Bondi MW: **Revision of the apolipoprotein E compensatory mechanism recruitment hypothesis**. *Alzheimers Dement* 2008, **4**(4):251-254.

68. Buckner RL, Sepulcre J, Talukdar T, Krienen FM, Liu H, Hedden T, Andrews-Hanna JR, Sperling RA, Johnson KA: **Cortical hubs revealed by intrinsic functional connectivity: mapping, assessment of stability, and relation to Alzheimer's disease**. *J Neurosci* 2009, **29**(6):1860-1873.

69. Hornung JP: **The human raphe nuclei and the serotonergic system**. *Journal of chemical neuroanatomy* 2003, **26**(4):331-343.

70. Mei H, Logothetis NK, Eschenko O: **The activity of thalamic nucleus reuniens is critical for memory retrieval, but not essential for the early phase of "off-line" consolidation**. *Learn Mem* 2018, **25**(3):129-137.

71. Griffin AL: **Role of the thalamic nucleus reuniens in mediating interactions between the hippocampus and medial prefrontal cortex during spatial working memory**. *Frontiers in systems neuroscience* 2015, **9**:29.

72. Hoover WB, Vertes RP: **Collateral projections from nucleus reuniens of thalamus to hippocampus and medial prefrontal cortex in the rat: a single and double retrograde fluorescent labeling study**. *Brain structure & function* 2012, **217**(2):191-209.

73. Ogundele OM, Lee CC, Francis J: **Thalamic dopaminergic neurons projects to the paraventricular nucleus-rostral ventrolateral medulla/C1 neural circuit**. *Anatomical record* 2017, **300**(7):1307-1314.

74. Brudzynski SM: **The ascending mesolimbic cholinergic system–a specific division of the reticular activating system involved in the initiation of negative emotional states**. *Journal of molecular neuroscience : MN* 2014, **53**(3):436-445.

75. Grootendorst J, Bour A, Vogel E, Kelche C, Sullivan PM, Dodart JC, Bales K, Mathis C: **Human apoE targeted replacement mouse lines: h-apoE4 and h-apoE3 mice differ on spatial memory performance and avoidance behavior**. *Behav Brain Res* 2005, **159**(1):1-14.

76. van Meer P, Acevedo S, Raber J: **Impairments in spatial memory retention of GFAP-apoE4 female mice**. *Behav Brain Res* 2007, **176**(2):372-375.

77. Raber J, Wong D, Buttini M, Orth M, Bellosta S, Pitas RE, Mahley RW, Mucke L: **Isoform-specific effects of human apolipoprotein E on brain function revealed in ApoE knockout mice: increased susceptibility of females**. *Proc Natl Acad Sci U S A* 1998, **95**(18):10914-10919.

78. Raber J, Wong D, Yu GQ, Buttini M, Mahley RW, Pitas RE, Mucke L: **Apolipoprotein E and cognitive performance**. *Nature* 2000, **404**(6776):352-354.

79. Hartman RE, Wozniak DF, Nardi A, Olney JW, Sartorius L, Holtzman DM: **Behavioral phenotyping of GFAP-apoE3 and -apoE4 transgenic mice: apoE4 mice show profound working memory impairments in the absence of Alzheimer's-like neuropathology**. *Exp Neurol* 2001, **170**(2):326-344.

80. Zerbi V, Wiesmann M, Emmerzaal TL, Jansen D, Van Beek M, Mutsaers MP, Beckmann CF, Heerschap A, Kiliaan AJ: **Resting-state functional connectivity changes in aging apoE4 and apoE-KO mice**. *J Neurosci* 2014, **34**(42):13963-13975.

81. Wiesmann M, Zerbi V, Jansen D, Haast R, Lutjohann D, Broersen LM, Heerschap A, Kiliaan AJ: **A Dietary Treatment Improves Cerebral Blood Flow and Brain Connectivity in Aging apoE4 Mice**. *Neural plasticity* 2016, **2016**:6846721.

82. Yin J, Turner GH, Coons SW, Maalouf M, Reiman EM, Shi J: **Association of amyloid burden, brain atrophy and memory deficits in aged apolipoprotein epsilon4 mice**. *Current Alzheimer research* 2014, **11**(3):283-290.

83. Guilfoyle DN, Gerum SV, Sanchez JL, Balla A, Sershen H, Javitt DC, Hoptman MJ: **Functional connectivity fMRI in mouse brain at 7T using isoflurane**. *Journal of neuroscience methods* 2013, **214**(2):144-148.

84. Gorges M, Roselli F, Muller HP, Ludolph AC, Rasche V, Kassubek J: **Functional Connectivity Mapping in the Animal Model: Principles and Applications of Resting-State fMRI**. *Front Neurol* 2017, **8**:200.

85. Jonckers E, Delgado y Palacios R, Shah D, Guglielmetti C, Verhoye M, Van der Linden A: **Different anesthesia regimes modulate the functional connectivity outcome in mice**. *Magn Reson Med* 2014, **72**(4):1103-1112.

86. Liang Z, King J, Zhang N: **Anticorrelated resting-state functional connectivity in awake rat brain**. *NeuroImage* 2012, **59**(2):1190-1199.

87. C. WG: **Pleiotropy, natural selection, and the evolution of senescence.** . *Evolution* 1957, **11**(4):398-411.

88. Alexander DM, Williams LM, Gatt JM, Dobson-Stone C, Kuan SA, Todd EG, Schofield PR, Cooper NJ, Gordon E: **The contribution of apolipoprotein E alleles on cognitive performance and dynamic neural activity over six decades**. *Biological psychology* 2007, **75**(3):229-238.

89. Marchant NL, King SL, Tabet N, Rusted JM: **Positive effects of cholinergic stimulation favor young APOE epsilon4 carriers**. *Neuropsychopharmacology* 2010, **35**(5):1090-1096.

90. Mondadori CR, de Quervain DJ, Buchmann A, Mustovic H, Wollmer MA, Schmidt CF, Boesiger P, Hock C, Nitsch RM, Papassotiropoulos A *et al*: **Better memory and neural efficiency in young apolipoprotein E epsilon4 carriers**. *Cereb Cortex* 2007, **17**(8):1934-1947.

91. Puttonen S, Elovainio M, Kivimaki M, Lehtimaki T, Keltikangas-Jarvinen L: **The combined effects of apolipoprotein E polymorphism and low-density lipoprotein cholesterol on cognitive performance in young adults**. *Neuropsychobiology* 2003, **48**(1):35-40.

92. Kunz L, Reuter M, Axmacher N, Montag C: **Conscientiousness is Negatively Associated with Grey Matter Volume in Young APOE varepsilon4-Carriers**. *Journal of Alzheimer's disease : JAD* 2017, **56**(3):1135-1144.

93. Wierenga CE, Clark LR, Dev SI, Shin DD, Jurick SM, Rissman RA, Liu TT, Bondi MW: **Interaction of age and APOE genotype on cerebral blood flow at rest**. *Journal of Alzheimer's disease : JAD* 2013, **34**(4):921-935.

94. Eisenberg DT, Kuzawa CW, Hayes MG: **Worldwide allele frequencies of the human apolipoprotein E gene: climate, local adaptations, and evolutionary history**. *American journal of physical anthropology* 2010, **143**(1):100-111.

95. Corbo RM, Ulizzi L, Scacchi R, Martinez-Labarga C, De Stefano GF: **Apolipoprotein E polymorphism and fertility: a study in pre-industrial populations**. *Molecular human reproduction* 2004, **10**(8):617-620.

96. van Exel E, Koopman JJE, Bodegom DV, Meij JJ, Knijff P, Ziem JB, Finch CE, Westendorp RGJ: **Effect of APOE epsilon4 allele on survival and fertility in an adverse environment**. *PLoS One* 2017, **12**(7):e0179497.

97. Jasienska G, Ellison PT, Galbarczyk A, Jasienski M, Kalemba-Drozdz M, Kapiszewska M, Nenko I, Thune I, Ziomkiewicz A: **Apolipoprotein E (ApoE) polymorphism is related to differences in potential fertility in women: a case of antagonistic pleiotropy?** *Proceedings Biological sciences / The Royal Society* 2015, **282**(1803):20142395.

98. Fujioka H, Phelix CF, Friedland RP, Zhu X, Perry EA, Castellani RJ, Perry G: **Apolipoprotein E4 prevents growth of malaria at the intraerythrocyte stage: implications for differences in racial susceptibility to Alzheimer's disease**. *Journal of health care for the poor and underserved* 2013, **24**(4 Suppl):70-78.

99. Aucan C, Walley AJ, Hill AV: **Common apolipoprotein E polymorphisms and risk of clinical malaria in the Gambia**. *Journal of medical genetics* 2004, **41**(1):21-24.

100. Wozniak MA, Faragher EB, Todd JA, Koram KA, Riley EM, Itzhaki RF: **Does apolipoprotein E polymorphism influence susceptibility to malaria?** *Journal of medical genetics* 2003, **40**(5):348-351.

101. Trumble BC, Stieglitz J, Blackwell AD, Allayee H, Beheim B, Finch CE, Gurven M, Kaplan H: **Apolipoprotein E4 is associated with improved cognitive function in Amazonian forager-horticulturalists with a high parasite burden**. *FASEB J* 2017, **31**(4):1508-1515.

Figures

Female WT vs Female APOE4

Brain Area	WT Mean	WT SD		APOE4 Mean	APOE4 SD	P Val
pontine reticular nucleus caudal	0.88	0.06	>	0.75	0.04	0.003
trapezoid body	0.13	0.01	>	0.11	0.01	0.004
gigantocellular reticular area	1.04	0.11	<	1.25	0.05	0.004
magnocellular preoptic nucleus	0.10	0.02	<	0.13	0.01	0.005
reuniens nucleus	0.18	0.01	>	0.16	0.01	0.011
triangular septal nucleus	0.05	0.02	<	0.09	0.01	0.012
2nd cerebellar lobule	0.91	0.07	>	0.80	0.02	0.013
CA2 hippocampus	0.13	0.01	<	0.15	0.01	0.014
medial dorsal thalamus	0.18	0.02	<	0.23	0.03	0.017
dorsal CA3 hippocampus	0.95	0.05	>	0.86	0.04	0.018
red nucleus	0.08	0.01	<	0.10	0.01	0.018
primary somatosensory ctx shoulder	0.21	0.01	>	0.14	0.05	0.019
principal sensory nucleus trigeminal	0.56	0.02	<	0.60	0.03	0.019
primary motor ctx	2.59	0.04	<	2.65	0.03	0.022
temporal ctx	0.41	0.09	>	0.31	0.02	0.031
5th cerebellar lobule	1.70	0.03	>	1.57	0.11	0.032
infralimbic ctx	0.45	0.02	>	0.39	0.05	0.039
ectorhinal ctx	0.23	0.02	<	0.29	0.05	0.039
primary somatosensory ctx forelimb	1.12	0.04	<	1.19	0.05	0.040
dorsal medial striatum	1.14	0.02	<	1.19	0.04	0.040
parvicellular reticular area	0.90	0.11	<	1.02	0.02	0.041
intercalated amygdala	0.03	0.01	<	0.04	0.01	0.044

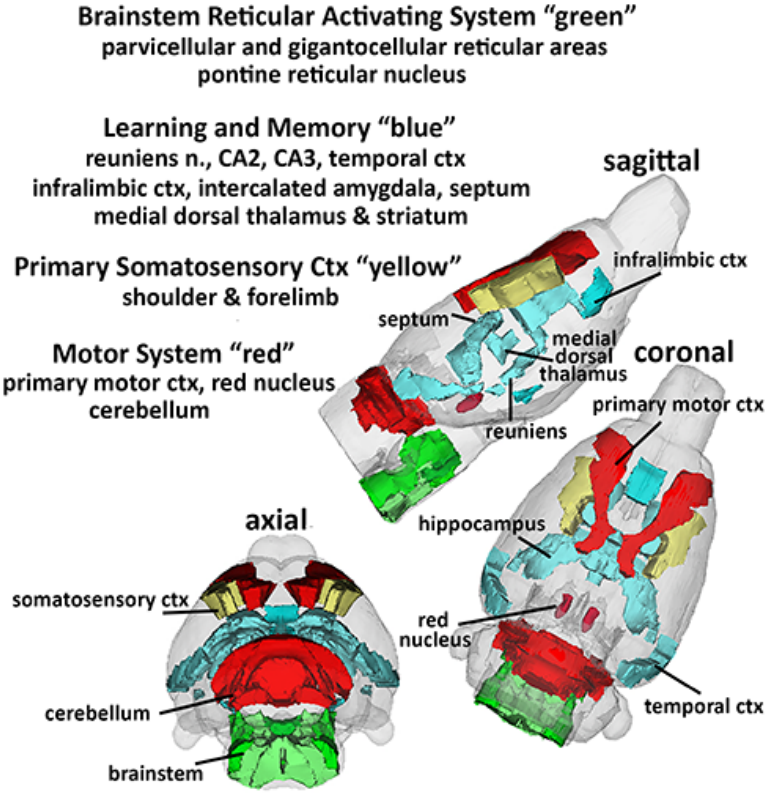

Figure 1

Differences in Brain Volumes. Tables showing significant differences in brain volumes (mm3) between genotypes and sexes are truncated from a list of 171 brain areas. The major differences are clustered into brain regions and presented as color coded 3D reconstructions in the glass brains to the right. SD = standard deviation. The p value for female WT vs female ε4 considering multiple comparisons is 0.025. The p value for female ε4 vs male ε4 is 0.020.

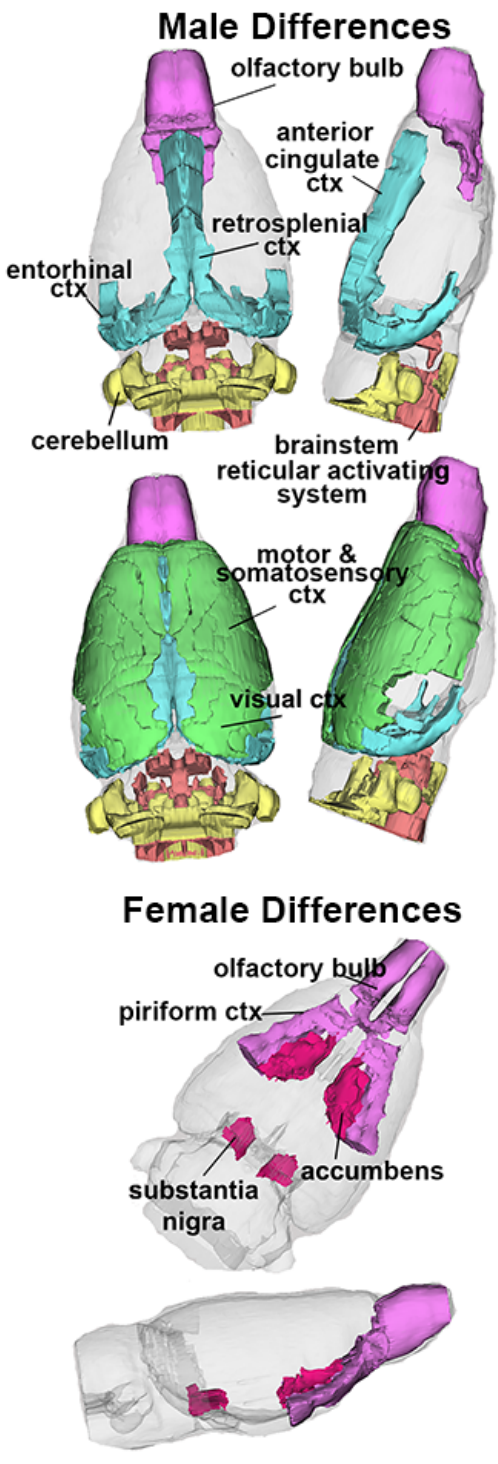

Male Fractional Anisotropy

Brain Area	Wild-Type Mean	SD		APOE4 Mean	SD	P val
secondary motor ctx	0.45	0.04	>	0.27	0.02	0.002
interposed nucleus	0.49	0.02	>	0.36	0.02	0.002
primary somatosensory ctx forelimb	0.41	0.03	>	0.29	0.01	0.004
primary motor ctx	0.45	0.05	>	0.29	0.01	0.004
frontal association ctx	0.40	0.03	>	0.27	0.02	0.005
entorhinal ctx	0.39	0.02	>	0.30	0.02	0.005
visual 1 ctx	0.45	0.04	>	0.29	0.03	0.007
medial cerebellar nucleus fastigial	0.54	0.03	>	0.37	0.04	0.008
secondary somatotsensory ctx	0.30	0.01	>	0.26	0.01	0.008
primary somatosensory ctx jaw	0.38	0.02	>	0.31	0.02	0.009
9th cerebellar lobule	0.53	0.04	>	0.34	0.04	0.010
copula of the pyramis	0.49	0.03	>	0.32	0.04	0.010
retrosplenial caudal ctx	0.44	0.04	>	0.32	0.02	0.014
gigantocellular reticular n. pons	0.48	0.03	>	0.32	0.04	0.015
vestibular nucleus	0.50	0.01	>	0.39	0.04	0.019
external plexiform layer	0.46	0.03	>	0.33	0.03	0.019
primary somatosensory ctx shoulder	0.43	0.05	>	0.29	0.02	0.020
primary somatosensory ctx barrel field	0.38	0.03	>	0.30	0.01	0.021
inferior olivary complex	0.48	0.02	>	0.22	0.08	0.021
glomerular layer	0.41	0.03	>	0.29	0.03	0.021
anterior cingulate area	0.40	0.03	>	0.31	0.02	0.025
visual 2 ctx	0.43	0.05	>	0.30	0.02	0.027
tenia tecta ctx	0.38	0.02	>	0.31	0.02	0.028
parietal ctx	0.45	0.06	>	0.32	0.02	0.029
habenula nucleus	0.39	0.04	>	0.30	0.02	0.030
locus ceruleus	0.52	0.02	>	0.40	0.04	0.030
primary somatosensory ctx hindlimb	0.42	0.06	>	0.29	0.02	0.032
granular cell layer	0.47	0.05	>	0.34	0.03	0.032
insular ctx	0.35	0.02	>	0.31	0.01	0.032
anterior olfactory nucleus	0.47	0.03	>	0.38	0.02	0.033
dorsomedial tegmental area	0.48	0.05	>	0.37	0.02	0.036
10th cerebellar lobule	0.48	0.04	>	0.31	0.06	0.036
parvicellular reticular area	0.49	0.03	>	0.35	0.05	0.036
primary somatosensory ctx upper lip	0.33	0.03	>	0.27	0.01	0.036
ventral subiculum	0.39	0.03	>	0.32	0.02	0.046

Female Fractional Anisotropy

Brain Area	Wild-Type Mean	SD		APOE4 Mean	SD	P val
granular cell layer	0.36	0.03	>	0.30	0.03	0.020
reticulotegmental nucleus	0.33	0.03	<	0.39	0.04	0.022
external plexiform layer	0.36	0.02	>	0.29	0.05	0.023
accumbens shell	0.31	0.05	<	0.38	0.01	0.034
rostral piriform ctx	0.28	0.04	<	0.34	0.03	0.045
substantia nigra compacta	0.39	0.03	<	0.45	0.04	0.050

Figure 2

Genotypic Differences in Fractional Anisotropy. The 2D axial images are probability maps for female □4 and male □4 as compared to their WT controls for fractional anisotropy. The data for the male □4 maps were generated from the table to the right. The major differences between the male and female genotypes are clustered into brain regions and presented as color coded 3D reconstructions. The p value for male WT vs male □4 is 0.044. SD = standard deviation

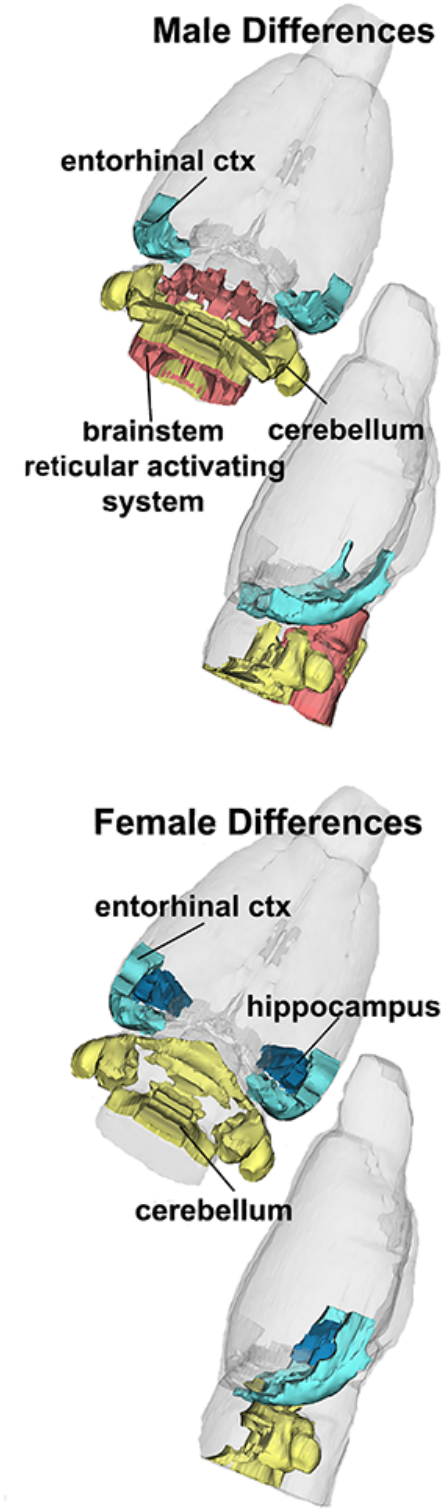

Male Apparent Diffusion Coefficient

Brain Area	Wild-Type Mean	SD		APOE4 Mean	SD	P val
parvicellular reticular area	2.91	0.09	>	2.07	0.11	0.000
gigantocellular reticular n. pons	2.94	0.17	>	2.05	0.13	0.002
raphe magnus	3.19	0.21	>	2.30	0.10	0.002
paraflocculus cerebellum	3.00	0.19	>	2.41	0.06	0.007
facial nucleus	3.14	0.21	>	2.33	0.16	0.009
inferior olivary complex	3.19	0.13	>	1.36	0.50	0.009
solitary tract nucleus	3.16	0.16	>	2.37	0.19	0.010
9th cerebellar lobule	3.26	0.13	>	2.28	0.26	0.010
principal sensory nucleus trigeminal	2.98	0.20	>	2.26	0.14	0.010
root of trigeminal nerve	3.19	0.23	>	2.43	0.15	0.013
copula of the pyramis	3.19	0.21	>	2.32	0.22	0.016
entorhinal ctx	3.21	0.28	>	2.51	0.08	0.016
8th cerebellar lobule	3.39	0.18	>	2.47	0.27	0.020
7th cerebellar lobule	3.57	0.20	>	2.85	0.19	0.023
trapezoid body	3.32	0.32	>	2.54	0.12	0.024
olivary nucleus	3.14	0.21	>	2.56	0.13	0.027
pontine reticular nucleus caudal	3.16	0.28	>	2.52	0.11	0.032
10th cerebellar lobule	3.10	0.20	>	2.10	0.34	0.033
periolivary nucleus	3.32	0.31	>	2.66	0.10	0.034
crus 2 of ansiform lobule	3.29	0.19	>	2.62	0.22	0.038
ectorhinal ctx	2.70	0.37	>	1.97	0.09	0.040
red nucleus	2.91	0.28	>	2.30	0.12	0.042
sub coeruleus nucleus	3.13	0.23	>	2.57	0.15	0.045
triangular septal nucleus	3.30	0.19	>	2.73	0.19	0.046
reticulotegmental nucleus	3.32	0.35	>	2.60	0.14	0.046
paramedian lobule	3.12	0.24	>	2.55	0.16	0.047

Female Apparent Diffusion Coefficient

Brain Area	Wild-Type Mean	SD		APOE4 Mean	SD	P val
3rd cerebellar lobule	2.41	0.07	>	2.22	0.09	0.006
lateral amygdaloid nucleus	3.44	0.55	>	2.55	0.14	0.016
copula of the pyramis	2.76	0.29	>	1.66	0.73	0.017
entorhinal ctx	2.57	0.19	>	2.02	0.35	0.018
tenia tecta ctx	2.78	0.17	>	2.52	0.02	0.019
7th cerebellar lobule	2.13	0.19	>	1.75	0.18	0.020
perirhinal ctx	2.28	0.14	>	2.05	0.08	0.023
white matter	2.36	0.07	>	2.25	0.05	0.033
9th cerebellar lobule	2.37	0.12	>	1.77	0.50	0.034
CA3 hippocampus ventral	2.34	0.11	>	2.17	0.08	0.035
flocculus cerebellum	2.60	0.23	>	2.05	0.41	0.036
CA1 hippocampus ventral	2.17	0.16	>	1.91	0.15	0.037
medial mammillary nucleus	2.43	0.29	<	3.07	0.48	0.041
10th cerebellar lobule	2.37	0.17	>	1.81	0.50	0.049

Figure 3

Genotypic Differences in Apparent Diffusion Coefficient. The 2D axial images are probability maps for female ε4 and male ε4 as compared to their WT controls for apparent diffusion coefficient. These data were generated from the tables to the right. The major differences between the male and female genotypes are clustered into brain regions and presented as color coded 3D reconstructions. The p value for female WT vs female ε4 considering multiple comparisons is 0.016. The p value for male WT vs male ε4 is 0.034. SD = standard deviation

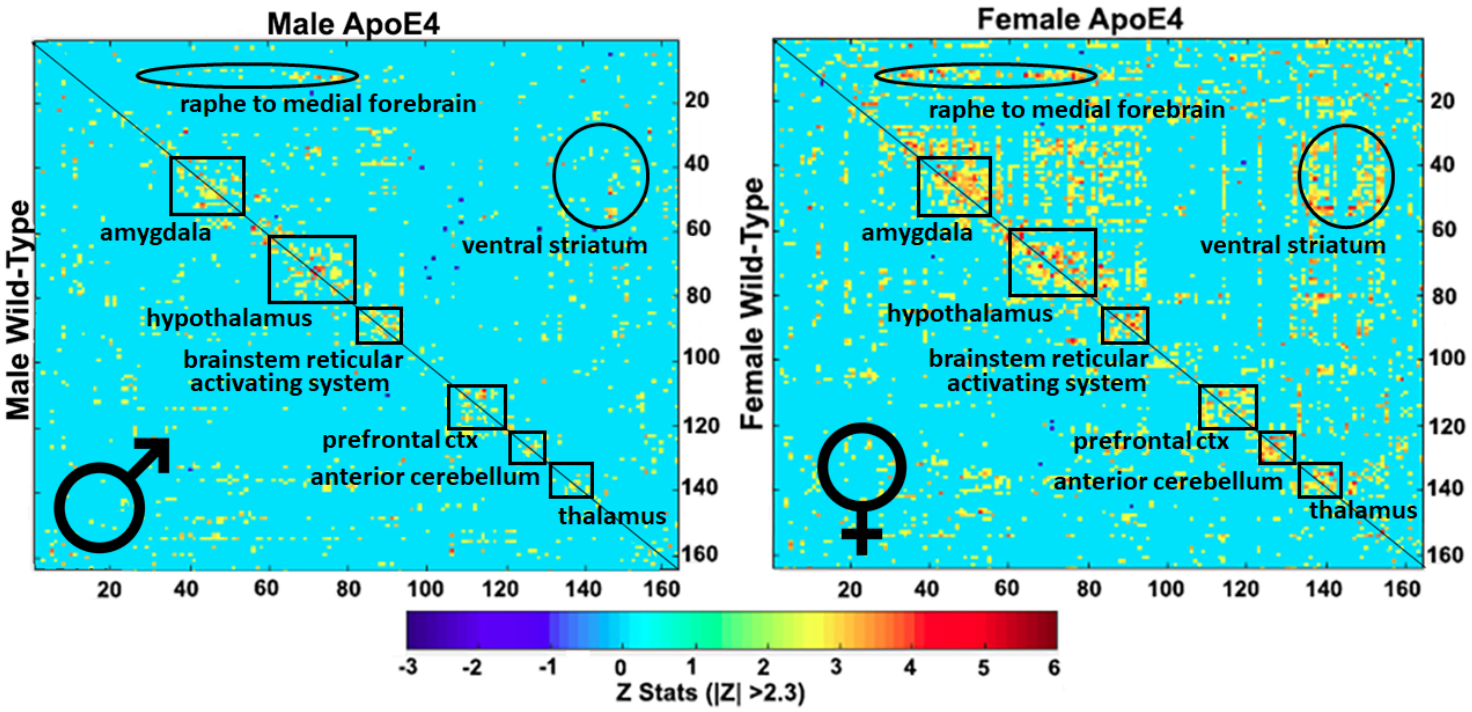

Figure 4

Genotypic Differences in Resting State Functional Connectivity. Shown are correlation matrices of 166 rat brain areas for rsFC comparing male ε4 vs male WT (n = 6) and female ε4 vs female WT (n = 6). Each dark red/yellow pixel represents one of 166 brain areas that is significantly correlated with other brain areas. The delineated brain areas with significant correlations appear as clusters because they are contiguous in their neuroanatomy and/or function. The diagonal line separates the genotypes. The location of the pixels for each genotype are a mirror image of each other. The female ε4 shows greater connectivity than the other genotypes.

Key Nodes				
raphe linear	reuniens nucleus	paraventricular nucleus hypothalamus	reticular nucleus midbrain	Connections
0.0191	**0.0027**	**0.0032**	0.0485	medial amygdala
0.0022	0.0579	0.5101	0.1199	lateral amygdala
0.0865	**0.0041**	0.0317	0.1187	basal amygdala
0.1301	0.0101	**0.0046**	0.2207	anterior amygdala
0.0196	0.0596	**0.0049**	0.4109	extended amygdala
0.0307	0.1144	NaN	**0.0009**	paraventricular hypothalamus
0.0045	0.4027	0.4890	**0.0036**	dorsal medial hypthalamus
0.0032	0.3954	0.2908	0.1018	posterior hypothalmus
0.0326	0.1193	**0.0059**	0.6254	ventral dentate hippocampus
0.1173	0.0149	**0.0032**	0.5547	ventral subiculum hippocampus
0.2104	**0.0015**	0.0136	**0.0014**	ventral pallidum, ventral striatum
0.7499	**0.0052**	0.0200	0.0277	olfactory tubercle
0.0001	0.1006	0.7388	**0.0006**	reticular tegmentum
0.7980	0.0134	**0.0009**	NaN	reticular area, midbrain
0.0505	**0.0045**	**0.0042**	0.9519	median raphe
0.3536	**0.0024**	0.2164	0.4197	pontine nucleus

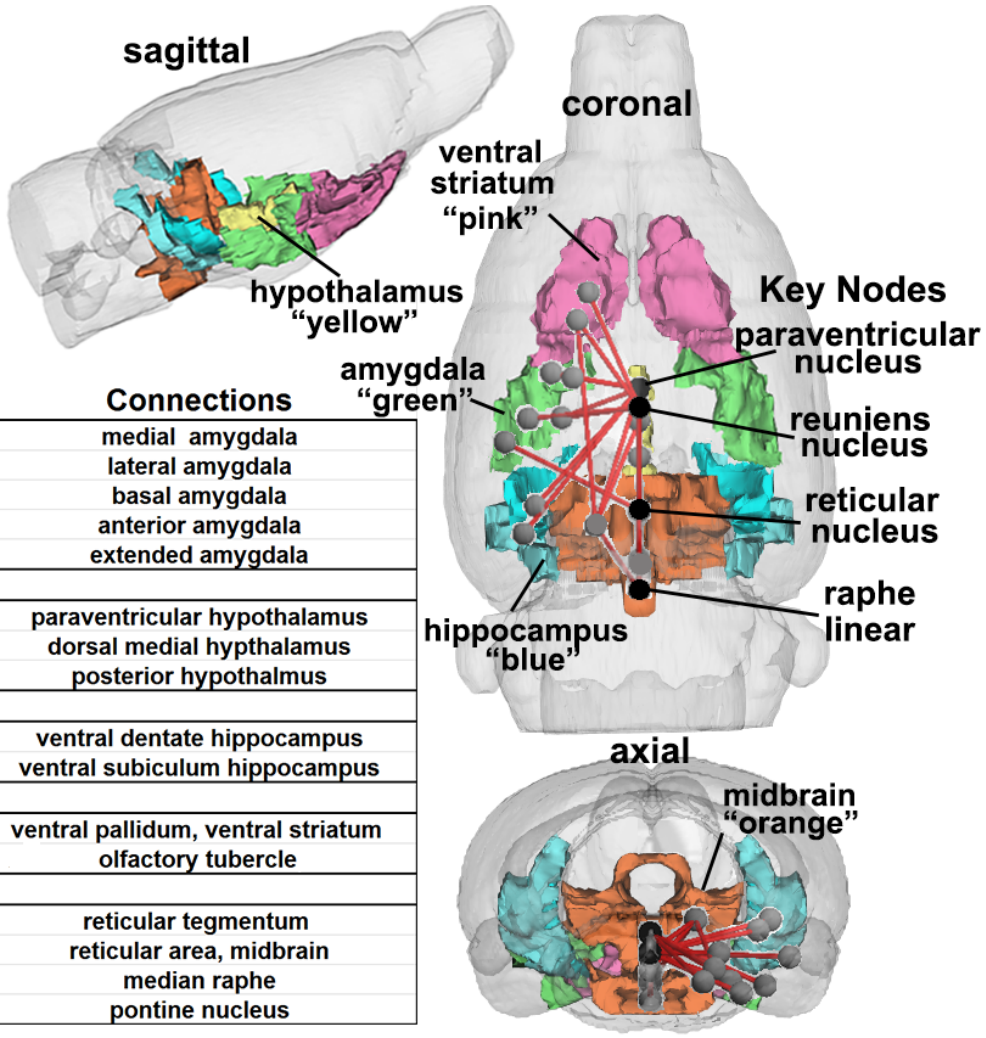

Figure 5

Key Nodes of Connectivity in Female 4. Shown are four key nodes in female 4 (n = 6) and a table of Z values to their connections (threshold 0.006). These integrated brain areas cluster around the amygdala, hypothalamus, hippocampus, ventral striatum, and midbrain/pontine reticular activating system. These brain areas are color coded and shown in 3D in the glass brain together with their connections to the four key nodes.

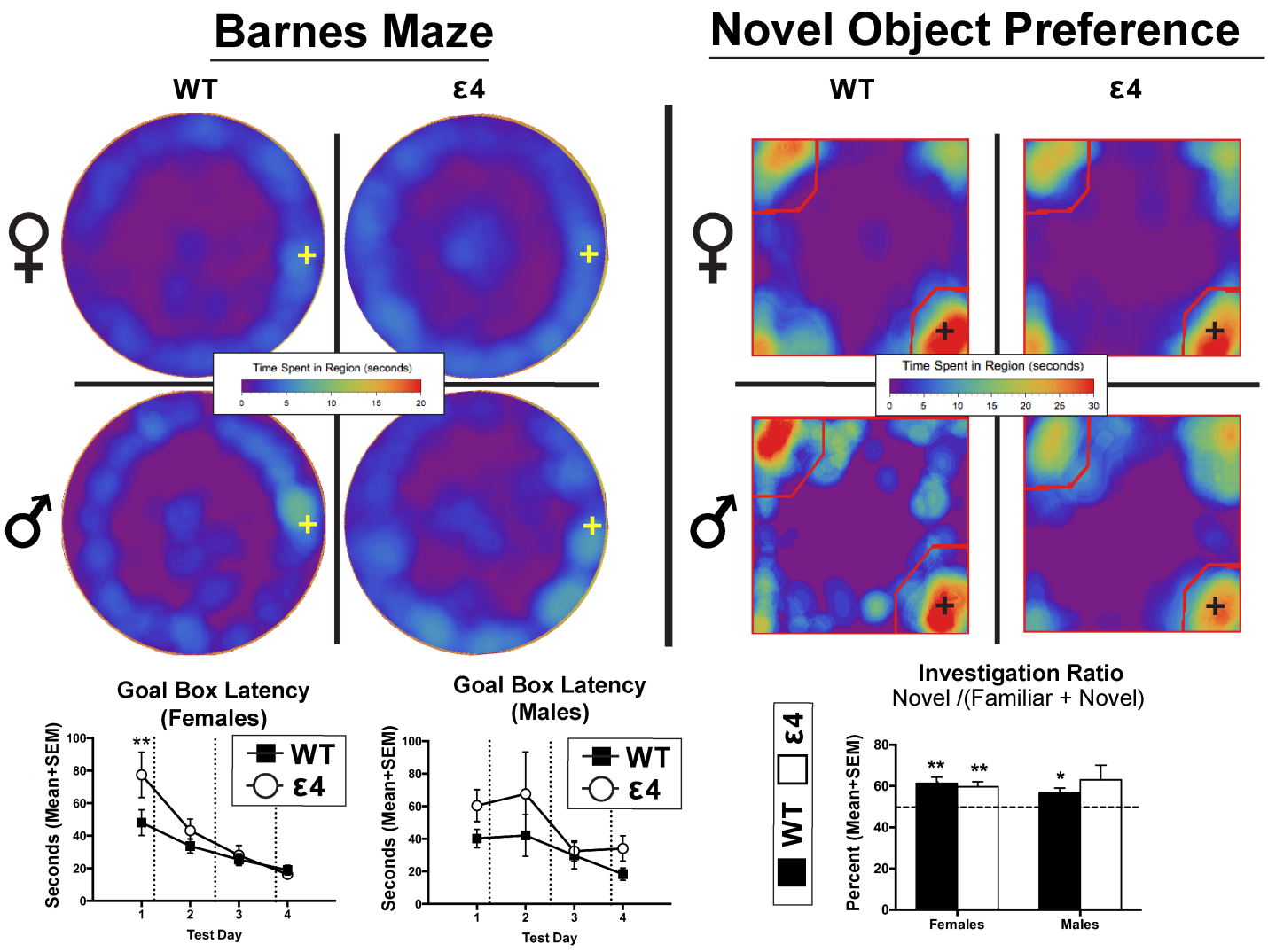

Figure 6

Genotypic Differences in Cognitive Behavior. Shown are data from Barnes maze and Novel Object Preference for female ε4 and male ε4 as compared to their WT controls. Search patterns for the Barnes maze goal box on the last day of testing showed no significant differences between genotypes but there was a significant main effect of genotype ($F(1,30) = 8.4$, $P < 0.01$) with both male and female ε4 rats showing longer Goal Box Latency across the four test days in comparison to their WT counterparts. The Path Efficiency Delta bar graph i.e. change in path efficiency from acquisition day 1 to day 4 was significant across groups ($F(3,30) = 4.58$, $P < 0.05$) driven by a difference between ε4 males and ε4 females ($t(15) = 3.31$, $P < 0.01$) where ε4 males became less efficient at finding the goal box, while ε4 females became more efficient over acquisition days. Heat maps for NOP show time for each genotype investigating the novel object. Qualitative data shows a pattern of exploration across genotypes with the greatest amount of time spent in proximity to the novel object indicated by the presence of red on the lower right corner of the maps. The Investigation Ratio bar graph shows all but ε4 males spent more time exploring the novel object beyond chance levels ($\bar{x}$ = 50% of the total testing time). The Total Time Exploring Novel Object bar graph shows a significant interaction between genotypes ($F(1,30) = 7.34$, $P <$

0.05) driven by a significant difference between WT and ε4 males (t(8) = 2.87, P < 0.01) Crosses on heat maps indicate goal box location and novel object location on the Barnes maze and NOR, respectively. * p < 0.05, ** p < 0.01.

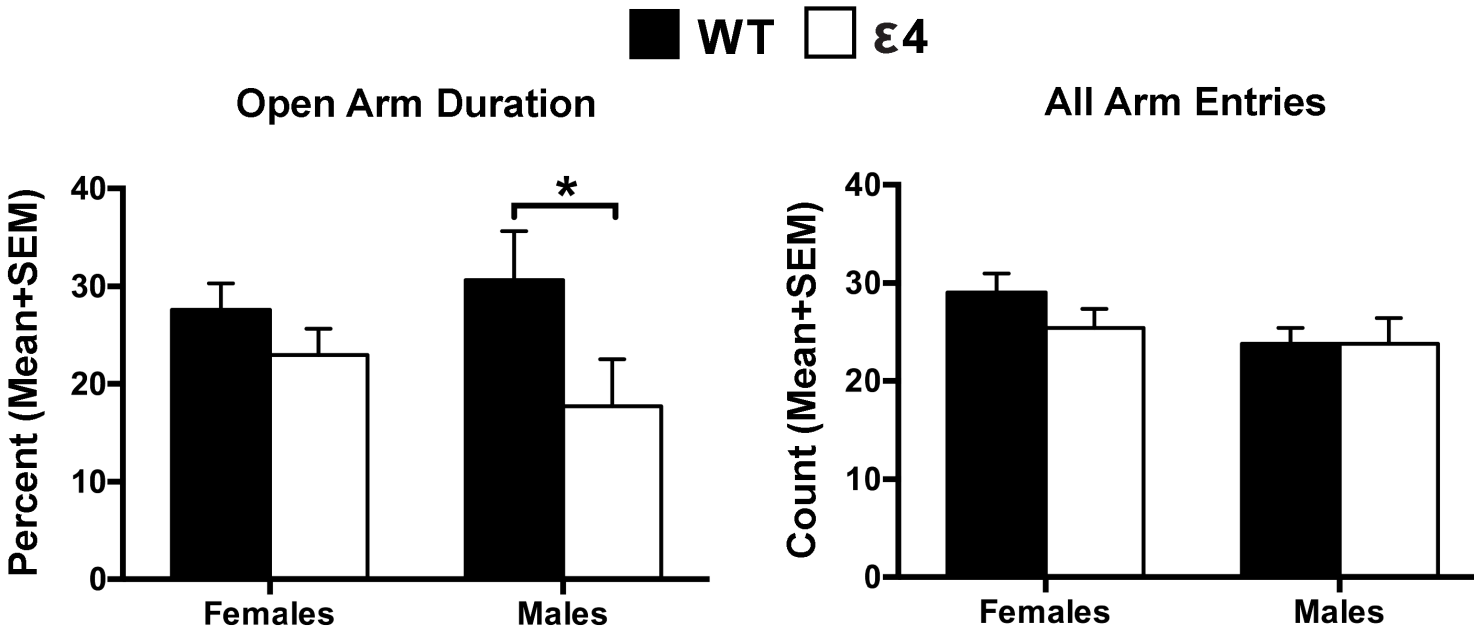

Figure 7

Elevated Plus Maze. Shown are data from the elevated plus maze for female ε4 and male ε4 as compared to their WT controls. ε4 males show more anxiety-like behavior (i.e., spent less time on the open arm) than their wildtype counterparts (p < 0.05).

Supplementary Files

This is a list of supplementary files associated with this preprint. Click to download.

- SupplementaryFig1BrainVolComparisons.tif
- SupplementaryTables6S13S.xlsx
- SupplementaryFig2BrainVolComparisons.tif
- SupplementaryTables2S5S.xlsx